

Reply to Topic Editor's decision and comments of 26 July 2020 on the paper "Predicting tidal heights for extreme environments: From 25 h observations to accurate predictions at Jang Bogo Antarctic Research Station, Ross Sea, Antarctica"

Do-Seong Byun¹, Deirdre E. Hart²

¹Ocean Research Division, Korea Hydrographic and Oceanographic Agency, Busan 49111, Republic of Korea

²School of Earth and Environment, University of Canterbury, Christchurch 8140, Aotearoa New Zealand

Correspondence to: Deirdre Hart (deirdre.hart@canterbury.ac.nz)

Format We are grateful for the Editor's final technical corrections on our paper. Below we reply to the individual comments (copied in blue), with a response, and then the final modified text.

Topic Editor Decision: Publish subject to technical corrections (26 Jul 2020) by Philip Woodworth

Comments to the Author: 26 July 2020

Remaining comments on this manuscript, mainly to do with describing the instruments again:

77 - thanks for clarifying the instruments. I think I would add 'absolute' and 'equivalent' to this to make it clear to the reader that this instrument is not measuring sea level as such i.e. "using a bottom-mounted absolute pressure sensor (WTG-256S AAT, Korea) with the data converted to equivalent sea level heights using the hydrostatic equation". That is, if I have understood you correctly.

- **Response:** This change has been made exactly as suggested.
- **This text now reads:** "using a bottom-mounted absolute pressure sensor (WTG-256S AAT, Korea) with the data converted to equivalent sea level heights using the hydrostatic equation"

218 - I would write this: Note that since the ROBT observation record was derived from a differential (vented) pressure sensor, unlike the absolute sensor at JBARS, and thus it affected by atmospheric (air pressure) forcing (i.e. S_a and S_{sa}).

- **Response:** This change has been made exactly as suggested.
- **This text now reads:** "Note that since the ROBT observation record was derived from a differential (vented) pressure sensor, and thus it includes proportionately large non-tidal (atmospheric) sea level variations, caution should be exercised in comparing the harmonic analysis results of the non-astronomical constituents, which are affected by atmospheric (air pressure) forcing (i.e. S_a and S_{sa})".

229-232 - you say now: "While these results elucidate an issue with predicting Ross Sea tides based on the diurnal and semidiurnal species alone, the aforementioned differences in gauge and record types in themselves can also result in different harmonic analysis results and, in turn, different prediction results". I guess you are now trying to accommodate the gauge type issue at line 77. Perhaps reword to be clearer if you agree but of course use your own words: "These results indicate one particular issue to do with long-period tides when predicting Ross Sea tides based on the diurnal and semidiurnal species alone. We note that the aforementioned differences in gauge records (subsurface pressure or real sea level) introduce another, in that, while diurnal and semidiurnal tides can be considered to be measured equivalently accurately, the longer-period components might be expected to instrument-dependent and so have uncertainties for the above experiments".

- **Response:** This change has been made as suggested.
- **This text now reads:** "These results elucidate one particular issue to do with long-period tides when predicting Ross Sea tides based on the diurnal and semidiurnal species alone. We note that the aforementioned differences in gauge records (subsurface pressure or real sea level) introduce another. That is, while the diurnal and semidiurnal tides might be considered to be measured equivalently accurately, the longer-period components are instrument-dependent and so have uncertainties for the above experiments".

419 - a one year-long observation

- **Response:** This change has been made exactly as suggested.
- **This text now reads:** "Table 2. Harmonic constants for 6 long-period tidal constituents, derived from harmonic analysis of a one year-long observation (2013) measured at the Cape Roberts sea level gauge (ROBT)".

Figure 6 - I think I would drop <Key> although up to you.

Response: We decided to keep the word <Key> in this figure.

Predicting tidal heights for extreme environments: From 25 hr observations to accurate predictions at Jang Bogo Antarctic Research Station, Ross Sea, Antarctica

Do-Seong Byun¹, Deirdre E. Hart²

¹Ocean Research Division, Korea Hydrographic and Oceanographic Agency, Busan 49111, Republic of Korea

²School of Earth and Environment, University of Canterbury, Christchurch 8140, Aotearoa New Zealand

Correspondence to: Deirdre E. Hart (deirdre.hart@canterbury.ac.nz)

Abstract. Accurate tidal height data for the seas around Antarctica are much needed, given the crucial role of these tides in the regional and global ocean, marine cryosphere, and climate processes. However obtaining long term sea level records for traditional tidal predictions is extremely difficult around ice affected coasts. This study evaluates the ability of a relatively new, tidal species based approach, the Complete Tidal Species Modulation with Tidal Constant Corrections (CTSM+TCC) method, to accurately predict tides for a temporary observation station in the Ross Sea, Antarctica, using a record from a neighbouring reference station characterised by a similar tidal regime. Predictions for the ‘mixed, mainly diurnal’ regime of Jang Bogo Antarctic Research Station (JBARS) were made and evaluated based on summertime (2017; and 2018 to 2019) short-term (25 hr) observations at this temporary station, along with tidal prediction data derived from year-long observations (2013) from the neighbouring ‘diurnal’ regime of Cape Roberts (ROBT). Results reveal the CTSM+TCC method can produce accurate (to within ~5 cm Root Mean Square Errors) tidal predictions for JBARS when using short-term (25 hr) tidal data from periods with higher than average tidal ranges (i.e. those at high lunar declinations). We demonstrate how to determine optimal short-term data collection periods based on the Moon’s declination and/or the modulated amplitude ratio and phase lag difference between the diurnal and semidiurnal species predicted from CTSM at ROBT (i.e. the reference tidal station). The importance of using long period tides to improve tidal prediction accuracy is also considered and, finally, the unique tidal regimes of the Ross Sea examined in this paper are situated within a wider Antarctic tidal context using FES2014 model data.

Copyright statement (will be included by Copernicus)

1 Introduction

Conventionally, year-long sea level records are used to generate accurate tidal height predictions via harmonic methods (e.g. Codiga, 2011; Foreman, 1977; Pawlowicz et al., 2002). Obtaining long term records for such tidal analyses is extremely difficult for sea ice affected coasts like that surrounding Antarctica. As a compliment to in situ tidal records, recent work has significantly advanced our understanding of tide models for the shallow seas around Antarctica and Greenland via the assimilation of laser altimeter data and use of Differential Interferometric Synthetic Aperture Radar (DInSAR) imagery, amongst other methods (Padman et al., 2008; 2018; King et al., 2011; Wild et al., 2019). However, Byun and Hart (2015) developed a new approach to successfully predict tidal heights based on as little as 25 hr of sea level records when combined with neighbouring reference site records, using their Complete Tidal Species Modulation with Tidal Constant Corrections (CTSM+TCC) method, on the coasts of Korea and New Zealand. Demonstrating the usefulness of this method for generating accurate tidal predictions for new sites on sea ice affected coasts is the motivation for this study. We focus on the Ross Sea, Antarctica, as our case study area.

Long-term, quality sea level records in the Ross Sea are few and far between, and include observations from gauges operated by New Zealand at Cape Roberts (ROBT); by the United States in McMurdo Sound (see reference to data in Padman et al., 2003); and by Italy at Mario Zucchelli Station (Gandolfi, 1996), all in the eastern Ross Sea. Permanent sea level gauge

installations in this extreme environment must accommodate or somehow avoid surface vents freezing over with sea ice, and damage to subsurface instruments from icebergs. There is also the challenge of securing and preventing damage to the cables that join the subsurface instruments to their onshore data loggers and power supplies, across the seasonally dynamic and harsh coastal and subaerial environments of Antarctic shorelines. At ROBT, these issues have been avoided by sheltering the sea level sensor towards the bottom of a 10 m long hole, drilled through a large shoreline boulder, from its surface ~2 m above the sea and sea ice level, to ~6 m below sea level, below the base of the sea ice (Glen Rowe, Technical Leader Sea Level Data, New Zealand Hydrographic Authority, *pers. comm.* 13 Dec. 2019). In the absence of a suitable permanent gauge site, hydrographic surveys have been conducted at the Korean Jang Bogo Antarctic Research Station (JBARS). Such surveys are best conducted during the summertime predominantly sea ice free window around mid-January to mid-February. Even then, mobile ice (Fig. 1) and severe weather events frequently hinder surveys via instrument damage or loss, not to mention the logistical difficulties of instrument deployment and recovery (Rignot et al. 2000). Accurate tidal records from the Ross Sea and other areas around Antarctica are thus scarce compared to those available from other regions, although these data are much needed given the crucial role of tidal processes around this continent (Han et al., 2005; Jourdain et al., 2018; Padman et al., 2003; 2018). Floating ice shelves occupy around 75% of Antarctica's perimeter (Padman et al., 2018). Tidal oscillations at the ice-ocean interface influence the location and extent of grounding zones (Padman et al., 2002), and control heat transfer and ocean mixing in cavities beneath the marine cryosphere (Padman et al., 2018) and the calving and drift of icebergs (Rignot et al. 2000). Tides also affect variability in polynyas; seasonal sea ice patterns; and thus the functioning of marine ecosystems. And tides affect the dynamics of landfast sea ice, which provides aircraft landing zones (Han and Lee, 2018). Accurate Antarctic region tide data are needed for models examining changes in global climate and ocean circulation (Han and Lee, 2018) while coastal tide data are needed for ice mass balance and motion studies (Padman et al., 2008; Rignot et al. 2000; Rosier and Gudmundsson, 2018). Ice thickness is typically measured by subtracting tidal heights from highly accurate but relatively low resolution (temporally or spatially) satellite or in situ observations of ice surface elevation (Padman et al., 2008). Where ice shelves and glacier tongues occur, grounding zone and ice flexure mechanics make ice thickness and motion determination challenging, so that accurate tidal height inputs are crucial (Wild et al. 2019). In this study, we tested the applicability of Byun and Hart's (2015) CTSM+TCC method in an extreme observation environment using 25 hr short-term records from JBARS, our temporary tidal observation station, and year-long data from ROBT, the neighbouring reference station. Sect. 2 of this paper details the JBARS and ROBT observation data sets used to generate harmonic tidal analysis results and CTSM+TCC tidal predictions. Sect. 3 explains how the CTSM+TCC method was applied and adapted in this case study (with Appendix 1 detailing the calculations), while Sect. 4 demonstrates the CTSM+TCC tidal prediction capability. Sect. 5 discusses the generation of fortnightly tide effects and double tidal peaks; and situates the Ross Sea tides examined in this paper within the wider context of Antarctic tidal regimes.

2 Antarctica's major tides: Observations and background

2.1 Study sites and data records

The Korea Hydrographic and Oceanographic Agency (KHOA) survey team went to JBARS in Northern Victoria Land's Terra Nova Bay, Ross Sea, Antarctica, in the austral summertime of 2017 (Fig. 2) for a preliminary fieldtrip to conduct hydrographic surveys and produce a nautical chart. This mission collected the first, 19 day sea level related record for JBARS: 10 min interval subsurface pressure observations were recorded between 28 Jan. and 16 Feb. 2017 using a bottom-mounted [absolute](#) pressure sensor (WTG-256S AAT, Korea) with the data converted to [equivalent](#) sea level heights using the hydrostatic equation. High-frequency sea level oscillations (<3 hr) were removed from the observation record using a fifth-order low-pass Butterworth filter. Note that the first and last days of this campaign comprised partial day records, so we excluded these end

134 days from our tidal prediction experiments, since our method requires continuous 25 hr input data (i.e. covering one tidal cycle
 135 minimum and, for convenience, starting at midnight). That left 17 days and 1 hour of useable tidal observation data as the basis
 136 of the primary JBARS observation record. Note that short-term records >25 hr may be used in CTSM+TCC but, as
 137 demonstrated in Byun and Hart (2015), large tidal range (range being twice amplitude) and high data quality have a much
 138 greater positive impact on prediction results than any increase in the length of the short-term observation records employed.
 139 For the purposes of a full-scale survey, three additional, discontinuous sea level observation records were measured by KHOA
 140 at JBARS between 29 Dec. 2018 and 11 Mar. 2019, all at 10 min intervals using the same instrument. Of these, the 20.54 day
 141 record produced between 29 Dec. 2018 and 18 Jan. 2019 comprised relatively high quality data with small residuals (i.e.
 142 observations minus predictions). We used this additional dataset (hereafter referred to as the JBARS 2019 observations) to
 143 verify CTSM+TCC method tidal predictions generated from input parameters derived from ‘daily’ (25 hr) slices of the 2017
 144 sea level records. Due to the short duration of the KHOA survey team’s forays into the Ross Sea, and in the absence of a
 145 permanent tide station at JBARS, it was not possible to collect the year-long sea level records that are commonly employed to
 146 obtain reliable tidal harmonic constants for tidal prediction.
 147 Approximately 269 km south of JBARS, there is a permanent tidal observation station named after its location on Cape Roberts
 148 (ROBT), operated by Land Information New Zealand (LINZ) and recording at intervals since November 1990 (Fig. 2). Five
 149 minute interval seawater pressure data have been collected at ROBT since November 2011 using GEOKON 4500 series
 150 Standard Piezometers, vented to the atmosphere, with this data converted to sea level heights using the hydrostatic equation.
 151 Part of the 2017 record from this site was unavailable online at the time of starting this research, so instead we chose as our
 152 reference records the 2013 ROBT sea level data, a quality year-long dataset with few missing points.

153 2.2 Tidal characteristic analyses and descriptions

154 Using the T_TIDE toolbox (Pawlowicz et al., 2002), we obtained the tidal harmonic constants of the 8 and 6 major tidal
 155 constituents for ROBT and JBARS, respectively (Table 1). Also the inference method was used to infer the P_1 constituent from
 156 the K_1 , and the K_2 constituent from the S_2 , with their amplitude ratios and phase lag differences obtained from harmonic
 157 analysis of the long-term ROBT reference station records. Analyses revealed that the two main diurnal (O_1 and K_1) and
 158 semidiurnal (M_2 and S_2) tides had similar amplitudes at the two stations, with the diurnal (semidiurnal) amplitudes being
 159 slightly larger (smaller) at ROBT than at JBARS, and the phase lags of all four tides having only slightly different values at
 160 the two stations. The amplitude differences result in slightly different tidal form factors at the two sites (e.g., F in Table 1).

161 3 Using the CTSM+TCC tidal prediction methodology in the Ross Sea

162 Having analysed the tidal harmonic constants at the two stations, we then employed the CTSM+TCC method (Byun and Hart,
 163 2015) to generate tidal height predictions for JBARS, our ‘temporary’ tidal observation station (subscript o), using ROBT as
 164 the ‘reference’ station (subscript r). This prediction approach (see Appendix 1 for the detailed calculations, and Byun and Hart
 165 (2015) for explanation of procedure development) is based on:

- 166 (i) using long-term (1 year, in our case) reference station records (LH_r) and CTSM calculations to make an initial
 167 anytime (τ) tidal prediction ($\eta_r(\tau)$), which involves summing tidal species’ heights for the reference station (Fig.3);
- 168 (ii) comparing the tidal harmonic constants (amplitude ratios and phase lag differences) of representative tidal
 169 constituents (e.g., M_2 and K_1) for each tidal species between the temporary and reference stations (Fig. 4), calculated
 170 using T_TIDE and concurrent short-term records (≥ 25 hr duration, starting at midnight) from the temporary (SH_o)
 171 and reference (SH_r) stations; and
- 172 (iii) using the step (ii) comparative data and the TCC calculations for each tidal species to adjust the $\eta_r(\tau)$ tidal species’
 173 heights in order to generate accurate, anytime tidal height predictions for the temporary tidal station ($\eta_o(\tau)$).

174 In this Ross Sea case study we used the 2017 JBARS tidal observation records (i.e. 17.04 days from 00:00 29 Jan. to 01:00 15
 175 Feb.) as a source of SH_o , keeping the second JBARS 2019 observation record for evaluation purposes.
 176 Importantly, this method assumes that the reference and temporary tidal stations are situated in neighbouring regimes with
 177 similar dominant tidal constituent and tidal species characteristics, and that the tidal properties between the two stations remain
 178 similar through time. As explained above, both JBARS and ROBT have tidal regimes that are primarily dominated by diurnal
 179 tides. LH_r can come from any time period, but must comprise high quality (e.g. few missing data) tidal height observations
 180 throughout.
 181 Byun and Hart (2015) recommended the use of short-term records gathered during periods of calm weather, to minimise errors
 182 due to atmospheric influences. They employed observational data for both SH_o and SH_r but as demonstrated in this paper the
 183 method can also be applied using tidal predictions as a source of SH_r . This adjustment in approach arose since for the 2017
 184 JBARS observation time period, the concurrent 2017 ROBT records available online (LINZ, 2019) had multiple missing data.
 185 We solved this issue by producing a year-long synthetic 2017 record for ROBT using T_TIDE (Pawlowicz et al., 2002) and
 186 the 2013 (i.e. LH_r) observational record as input data. The 17.04 days of predicted tides that were concurrent with the 2017
 187 JBARS observation record were then used as our SH_r source. While this CTSM+TCC method adjustment was procedurally
 188 small, it represents an important adaptation in the context of generating tidal predictions for stations situated in extreme
 189 environments, since concurrent temporary and reference station observations might be rare in such contexts.
 190 When using CTSM+TCC, if the available temporary tidal station observation record covers multiple days, it is best practice
 191 to experiment by generating multiple $\eta_o(\tau)$, each using different concurrent pairs of SH_o and SH_r daily data slices in step (ii)
 192 above, to produce daily amplitude ratios and phase lag differences between the two stations for the diurnal K_1 and semidiurnal
 193 M_2 tidal constituents. Comparisons are then made between the different $\eta_o(\tau)$ data sets produced and the original temporary
 194 station observations, to determine the optimal 25 hr window to use: once selected, tidal height predictions can be generated
 195 for the temporary observation station for any time period. Thus, 17 individual 25 hr duration data slices were clipped from the
 196 2017 JBARS observation records and from the concurrent ROBT predictions, forming 17 pairs of SH_o and SH_r ‘daily’ slices.
 197 Each paired data set was then used with LH_r to generate tidal height predictions for JBARS covering both the 2017 and 2019
 198 KHOA observation campaign time periods. Comparisons were made between the complete JBARS observations and the 17
 199 prediction data sets generated for each campaign to identify which 25 hr short-term data window produced optimal $\eta_o(\tau)$
 200 results.

201 4 Results

202 4.1 Tidal prediction evaluation

203 CTSM+TCC was used to produce 17 different JBARS tidal prediction data sets for the period 29 Jan. to 14 Feb. 2017, based
 204 on harmonic analysis results of the ‘daily’ (25 hr) K_1 and M_2 amplitudes and phase lags at our two tidal observation stations.
 205 Figure 5a illustrates one such tidal height prediction data set, in comparison to the observed tides. In order to evaluate the 17
 206 different prediction results, each prediction data set was compared with the concurrent JBARS field observations via Root
 207 Mean Square Error (RMSE) and coefficient of determination (R^2) statistics.
 208 RMSEs between the 2017 observations and predictions ranged from 4.26 cm to 20.56 cm, while R^2 varied from 0 to 0.94,
 209 across the 17 ‘daily’ experiments (Fig. 6). Eleven of the experiments produced accurate results (i.e. excluding those derived
 210 from 31 Jan.; and 1 to 4 and 14 Feb. data slices). Daily datasets from periods with relatively high tidal ranges (>83.5 cm)
 211 produced predictions with RMSEs <5 cm and R^2 values >0.92 . The maximum tidal range occurred on 9 Feb., with step (ii)
 212 data slices from this date producing predictions with a low (but not the lowest) RMSE (4.81 cm). The predictions with the
 213 lowest RMSE (4.259 cm) and highest R^2 value (0.941) were produced using data slices from one day earlier, 8 Feb. 2017 (Fig.
 214 5a and Fig. 6). In contrast to the successful prediction datasets, that based on using the 2 Feb. 2017 data slices in step (ii) of

the method produced predictions with very high RMSE (20.56 cm) and very low R^2 (0.00) values (Fig. 6). The 2 Feb. 2017 tides were characterised by the smallest tidal range (11.95 cm) of the JBARS record, during a period of low lunar declination. Interestingly, RMSEs and R^2 values between the 2019 CTSM+TCC tidal predictions and observations were almost identical to those of the 2017 comparisons, revealing that our approach performed consistently across different prediction years. As in the 2017 experiments, the 2019 prediction dataset made using the 8 Feb. 2017 data slices (i.e., in step (ii) of the method) produced the lowest RMSE (5.3 cm) and highest R^2 (0.913) values of the 2019 experiments (Fig. 5b). Across both the 2017 and 2019 prediction time periods, the RMSE and R^2 results varied in relation to the JBARS tidal range, with greater accuracy evident in predictions made using step (ii) 2017 data slices from periods with above average tidal ranges. In the JBARS area of the Ross Sea during the 2017 short-term observation period, above average tidal ranges corresponded to the period when the moon was near its greatest northern declination (Fig. 6). Collectively these results show that the CTSM+TCC method can be used successfully to predict tidal heights for JBARS, when using short-term observation records gathered from periods at high lunar declination, and thus above average tidal ranges, with relatively calm weather, together with observation or prediction records from the neighbouring reference station ROBT.

4.2 Determining the ideal short-term sea level observation period when using CTSM+TCC

The previous section verified that the CTSM+TCC method can be used to generate accurate tidal predictions based on 25 hr sea level records, from periods with above average tidal ranges, for a temporary station in a mixed, mainly diurnal regime and a reference station in a diurnal regime. The question arises as to how to determine optimal observation days in such settings to produce the most accurate tidal predictions.

For semidiurnal or mixed, mainly semidiurnal tidal regimes, we can estimate preferred temporary station observation days, those with the largest tidal ranges, based on the moon's phase, without reference to tide tables. That is, spring tides commonly occur just a day or two after the full and new moon, which reoccurs at a period of 14.76 days. The time lag between the full or new moon and the spring tide is called the age of the tide (AT).

Similarly, in a diurnal tide regime or a mixed, mainly diurnal tide regime, preferred temporary station observation days can be estimated based on the lunar declination (Fig. 7), which varies at a period of 13.66 days. That is, maximum tidal range days can be estimated for JBARS based on the day of the Moon's greatest northern (GN) and southern (GS) declinations. The time between the Moon's semi-monthly GN and GS declinations and their effects on tidal range, called the age of diurnal inequality (ADI), is commonly 1 to 2 days. The GN and GS lunar declinations during our temporary station summertime observation periods occurred on 8 Feb. 2017 (GN) and on 6 Jan. 2019 (GS) respectively (Fig. 7), with the maximum diurnal tides at JBARS expected around 1 day after each lunar declination peak.

Thus, when planning to use the CTSM+TCC tidal prediction method for places characterised by diurnal or mixed, predominantly diurnal tidal regimes, we can use knowledge of the moon's declination to select potential sea level observation days.

4.3 Comparison of ROBT and JBARS tidal species characteristics

The CTSM+TCC tidal prediction method is based on the assumption that the tidal harmonic characteristics of each tidal species are very similar between the temporary and reference stations. This is because the reference station tidal species' CTSMs form the basis of the tidal predictions for the temporary observation station. To test the validity of this assumption, we examined the phase lag (G) differences of the two major diurnal and semidiurnal tidal constituents using ADI and AT , calculated as:

$$ADI \text{ (day)} = \left(\frac{G_{K_1} - G_{O_1}}{\omega_{K_1} - \omega_{O_1}} \right) / 24, \text{ and} \quad (1)$$

$$AT \text{ (day)} = \left(\frac{G_{S_2} - G_{M_2}}{\omega_{S_2} - \omega_{M_2}} \right) / 24, \quad (2)$$

where ω_{K_1} ($= 15.0410686^\circ \text{ hr}^{-1}$), ω_{O_1} ($= 13.9430356^\circ \text{ hr}^{-1}$), ω_{S_2} ($= 30.0000000^\circ \text{ hr}^{-1}$), and ω_{M_2} ($= 28.9841042^\circ \text{ hr}^{-1}$) are the angular speeds of the K_1 , O_1 , S_2 and M_2 tides, respectively. Results revealed that the *ADI* are very similar, and there is <1 day *AT* difference, between ROBT and JBARS respectively (Table 1), indicating that the tidal characteristics of the representative tidal constituents for each species between the two stations are very similar, in particular the dominant diurnal species. Note that the negative *AT* values in Table 1 are an unusual feature of the Ross Sea tides, given that elsewhere spring tides commonly occur a day or two after the full and new moon. The *ADI* and *AT* similarities between our two stations explain why we found the CTSM+TCC method successful in generating the Ross Sea tidal predictions.

5 Discussion

5.1 Explaining fortnightly tide effects and double tide peaks in the Ross Sea tidal predictions

We have demonstrated that the CTSM+TCC approach can produce reasonably accurate tidal predictions ($\text{RMSE} < 5 \text{ cm}$, $R^2 > 0.92$) for a new site in the Ross Sea, Antarctica, based on 25 hr temporary station observation records from periods with above average tidal ranges, plus neighbouring reference station records. Our results compare favourably with those of Han et al. (2013), who reviewed the tidal height prediction accuracy of 4 models for Terra Nova Bay, Ross Sea: these models generated similar quality results to our CTSM+TCC results, with R^2 values between 0.876 and 0.907, and RMSEs ranging from 3.6 to 4.1 cm. However, as shown in Fig. 5, our results contain a changing fortnightly timescale bias in estimates. This error pattern likely resulted from our application of CTSM+TCC considering only 2 major tidal species (diurnal and semidiurnal) whilst ignoring several long period and small amplitude short period tides.

Table 2 summarises the characteristics of 6 long-period tides (S_a , S_{sa} , MS_m , M_m , M_f , MS_f) at the ROBT station, derived from tidal harmonic analysis of year-long (2013) in situ observation records. Note that since the ROBT observation record was derived from [a differential \(vented\) seawater pressure sensor measurement](#), and thus [it](#) includes proportionately large non-tidal (atmospheric) sea level variations, caution should be exercised in comparing the harmonic analysis results of the non-astronomical constituents, which are affected by [seawater density and atmospheric \(air pressure\)](#) forcing (i.e. S_a and S_{sa}).

To investigate the main cause of the apparent fortnightly prediction biases in our results, we examined the effects of two fortnightly tidal constituents (M_f , and MS_f) at ROBT using T_TIDE. Three 2019 tidal prediction experiments were conducted:

- *Srun* excluded all long-period tides (see list of exclusions in Table 2);
- *Run1* was based on *Srun* but also incorporated M_f ; and
- *Run2* was based on *Srun* but also incorporated M_f and MS_f ;

with T_TIDE predictions made for each case. Comparisons between *Run1* and *Srun* predictions revealed that exclusion of the M_f tide (2.7 cm amplitude) can produce prediction biases during periods of lunar declination change, with comparisons between *Run2* and *Run1* results revealing that the additional exclusion of the MS_f tide (1.2 cm amplitude) intensifies the biases. [While these results elucidate one particular an-issue to do with long-period tides when predicting Ross Sea tides based on the diurnal and semidiurnal species alone, We note that the aforementioned differences in gauge and records types \(subsurface pressure or real sea level\) introduce another. That is, while the diurnal and semidiurnal tides might be considered to be in-themselves can-measured equivalently accurately, the longer-period components are expected to be instrument-dependent and so have uncertainties for the above experiments also result in different harmonic analysis results and, in turn, different prediction results.](#) Rosier and Gudmundsson (2018) found that ice flows are modulated at various tidal frequencies, including that of the MS_f tide. However, because these tides' amplitudes have small signal-to-noise ratios (<1) with large standard errors (Table 2), caution should be exercised when elucidating fortnightly tide effects using these constituents. Nevertheless, studies indicate that incorporating major and minor tidal constituents, including long period tides, into tidal predictions may be advantageous for their use in ice flow and ice-ocean front modelling specifically (e.g. Rignot et al., 2000; Rosier and Gudmundsson, 2018).

294 Consideration of additional, long period tides in predictions is one recommendation we have for future work on improving
 295 tidal predictions for Ross Sea coasts.

296 Another characteristic of our results needing explanation is the double tidal peaks evident in both the tidal observations and
 297 predictions at JBARS. These peaks occur, for example, in Fig. 5b between Jan. 11th and 17th, 2019. To explore why these
 298 double peaks occur, we generated JBARS tidal height predictions using Eq. (A1) and the 2019 tidal constants listed in Table
 299 1 for the two major diurnal and semidiurnal tides. Fig. 8a shows separately the resulting diurnal (with their period of 13.66
 300 days) and semidiurnal (with their period of 14.77 days) species' tide predictions. The combination of these out-of-phase tidal
 301 species generates double peaks (or double troughs) around low and high tide (Fig. 8b) for periods when the diurnal tide
 302 amplitude is low, due to the similar amplitude K_1 and O_1 tides cancelling each other out across a fortnight, allowing the
 303 combined M_2 and S_2 amplitude to temporarily approach or exceed that of the combined K_1 and O_1 tides (Fig. 8c). Since the
 304 semidiurnal tides are slightly stronger, and the diurnal tides are slightly weaker, at JBARS compared to at ROBT (Table 1),
 305 these double tide peaks occur more commonly at JBARS.

306 5.2 Understanding the contrasting tidal environments around Antarctica

307 Figure 9 illustrates the form factors of tidal regimes in the seas surrounding Antarctica, according to FES2014 model data.
 308 There are large areas characterised by diurnal ($F > 3$); mixed, mainly diurnal ($1.5 < F < 3$); and mixed, mainly semidiurnal
 309 ($0.25 < F < 1.5$) forms. Only in a small area half-way along the Weddell Sea coast of the Antarctic Peninsula (at 72°S) do tides
 310 exhibit a semidiurnal form ($F < 0.25$). The Weddell Sea is dominated by mixed, mainly semidiurnal tides, excepting the
 311 semidiurnal area mentioned and another small area exhibiting diurnal tides ($F > 3$) at around 76.5°S, where amphidromic points
 312 (i.e. zero amplitudes) occur for both the M_2 and S_2 tides. Strong diurnal tides predominate in the Ross Sea area of West
 313 Antarctica, around to the Amundsen Sea. In addition, a small area near Prydz Bay (Fig. 2) in East Antarctica exhibits diurnal
 314 and mixed mainly diurnal tides. The rest of the seas surrounding Antarctica are predominantly characterised by mixed, mainly
 315 semidiurnal tides.

316 Since diurnal tides have larger nodal amplitude factor and nodal angle variations than semidiurnal tides (Pugh and Woodworth,
 317 2014), areas like the Ross Sea will have larger variations in tidal height across the 18.61 year lunar nodal cycle compared to
 318 areas like the Weddell Sea. As the nodal amplitude factor variations of the diurnal and semidiurnal tides are out of phase, this
 319 leads to differing tidal responses around Antarctica over 18.61 years, particularly between the Ross and Weddell Seas (see
 320 details for ROBT in Byun and Hart, 2019). Given that CTSM+TCC is based on modulated tidal amplitude and phase lag
 321 corrections for each diurnal and semidiurnal species, this approach is applicable in studying a continent with such a diversity
 322 of tidal regime types.

323 6 Conclusions

324 This paper has demonstrated the usefulness of the CTSM+TCC method for tidal prediction in extreme environments, where
 325 long-term tidal station installations are difficult, using the Ross Sea in Antarctica for our case study. Here CTSM+TCC
 326 methods can be employed for accurate tidal height predictions for a temporary tidal observation station using short-term (≥ 25
 327 hr) sea level records from this site, plus long-term (1 year) tidal records from a neighbouring reference tidal station. Essentially
 328 the temporary and reference station sites must share similarities in their main tidal constituent and tidal species characteristics
 329 for CTSM+TCC to produce acceptable results.

330 Using this approach, an initial tidal prediction time series is generated for the temporary station using CTSM and the reference
 331 station long-term records. The temporary station predicted time series can then be adjusted via TCC of each tidal species,
 332 based on harmonic comparisons between the short-term temporary station observation record and its corresponding modelled

333 predictions, leading to improved accuracy in the tidal predictions. The modulated amplitude ratio and phase lag difference
334 between diurnal and semidiurnal species predicted from CTSM at the reference station can be used as an indicator for selecting
335 optimal short term observation dates at a temporary tidal station.
336 This paper has further demonstrated that the CTSM+TCC approach can be employed successfully in the absence of concurrent
337 short-term (25 hr) records from the reference station, since a tidal harmonic prediction program can be used to produce a
338 synthetic short-term record for the reference station, based on a quality long-term (1 year) record from that site.
339 The proper consideration of long-period tides in the CTSM+TCC approach remains a challenge, as outlined in this study, with
340 the solutions to this issue likely to improve tidal predictions further. However, this study demonstrates that the CTSM+TCC
341 method can already produce tidal predictions of sufficient accuracy to aid local polar station maritime operations, as well as
342 starting to help resolve gaps in the spatial coverage of tidal height predictions for scientists studying important issues, such as
343 the rate and role of ice loss along polar coastlines.

344 **Code Availability**

345 The T_TIDE based CTSM code is available from https://au.mathworks.com/matlabcentral/fileexchange/73764-ctsm_t_tide.

346 **Data Availability**

347 The sea level data used in this paper are available from LINZ (2019) for selected ROBT records, with the remaining ROBT
348 records available by email application (customersupport@linz.govt.nz); and the JBARS records used are available on request
349 from KHOA (infokhoa@korea.kr). Details of the FES2014 tide model are found in Carrère et al. (2016) and via
350 <https://www.aviso.altimetry.fr/en/data/products/auxiliary-products/global-tide-fes.html>.

351

352 Appendix 1

353 This appendix describes the calculations involved in using the CTSM+TCC approach as employed in this Ross Sea, Antarctica,
354 case study. For a fuller description of the development of this approach and its application in semidiurnal and mixed, mainly
355 semidiurnal tidal regime settings, see Byun and Hart (2015).

356 As explained in the main body of this paper, we used 25 hr slices of the 2017 short-term observations from JBARS (SH_o), our
357 temporary tidal observation station (subscript *o*), and 2013 year-long observations (LH_r) and 2017 short-term tidal predictions
358 (SH_r, concurrent with SH_o) from ROBT, our reference tidal station (subscript *r*), as the basis of JBARS tidal prediction
359 calculations. We then employed the full 17.04 day 2017 JBARS tidal observation data set, and an additional 21.54 day 2019
360 JBARS tidal observation dataset, to evaluate the success of the CTSM+TCC tidal prediction calculations for this site.

361 The CTSM+TCC, expressed as the summation of each tidal species cosine function, includes three key steps:

- 362 (i) calculating each tidal species' modulation at the reference tidal station;
- 363 (ii) comparing the tidal harmonic constants between the temporary observation and reference stations (e.g., the tidal
364 amplitude ratios and phase lag differences of each representative tidal constituent for each tidal species calculated
365 from concurrent observation records between two stations); and
- 366 (iii) adjusting the tidal species modulations calculated in the first step using the correction factors calculated in the
367 second step to produce predictions for the temporary tidal station.

368 As a first step, tidal height predictions for the temporary station ($\eta_o(\tau)$) were initially derived from reference station predictions
369 ($\eta_r(\tau)$) on the assumption that the tidal properties between the two stations remain similar through time. Using the modulated
370 amplitude ($A_r^{(s)}$) and the modulated phase lag ($\varphi_r^{(s)}$) for each tidal species, this step is expressed as:

$$371 \eta_r(\tau) = \sum_{s=1}^k A_r^{(s)}(\tau) \cos(\omega_R^{(s)} t - \varphi_r^{(s)}(\tau)) \quad (A1)$$

372 with

$$373 A_r^{(s)}(\tau) = \sqrt{\sum_{i=1}^m [f_i^{(s)}(\tau) a_i^{(s)}]^2 + 2 \sum_{i=1}^{m-2} \sum_{j=i+1}^m [f_i^{(s)}(\tau) a_i^{(s)}] [f_j^{(s)}(\tau) a_j^{(s)}] \cos\{(\omega_i^{(s)} - \omega_j^{(s)}) t + [V_i^{(s)}(t_0) + u_i^{(s)}(\tau) - G_i^{(s)}] - [V_j^{(s)}(t_0) + u_j^{(s)}(\tau) - G_j^{(s)}]\}}$$

374 (A2)

375 and

$$376 \varphi_r^{(s)}(\tau) = \tan^{-1} \left(\frac{\sum_{i=1}^m f_i^{(s)}(\tau) a_i^{(s)} \sin[(\omega_i^{(s)} - \omega_R^{(s)}) t + V_i^{(s)}(t_0) + u_i^{(s)}(\tau) - G_i^{(s)}]}{\sum_{i=1}^m f_i^{(s)}(\tau) a_i^{(s)} \cos[(\omega_i^{(s)} - \omega_R^{(s)}) t + V_i^{(s)}(t_0) + u_i^{(s)}(\tau) - G_i^{(s)}]} \right) \quad (A3)$$

377 where superscript *s* denotes the type of tidal species (e.g., 1 for diurnal species and 2 for semidiurnal species); *m* is the number
378 of tidal constituents; *t*₀ is the reference time; *t* is the time elapsed since *t*₀; and $\tau = t_0 + t$; $\omega_i^{(s)}$ are the angular frequencies
379 of each tidal constituent (subscripts *i* and *j*); $\omega_R^{(s)}$ are the angular frequencies of each tidal constituent representing a tidal
380 species (subscript *R*); with the dominant tidal constituent of each tidal species used as the representative for that species (e.g.,
381 K₁ and M₂ are used as representative of the diurnal and semidiurnal species, respectively). For each tidal constituent, $a_i^{(s)}$ and
382 $G_i^{(s)}$ are the tidal harmonic amplitudes and phase lags (referenced to Greenwich); $f_i^{(s)}(\tau)$ is the nodal amplitude factor of each
383 tidal constituent; $u_i^{(s)}(\tau)$ is the nodal angle; and $V_i^{(s)}(t_0)$ is the astronomical argument. T_TIDE was used for tidal harmonic
384 analysis as well as for calculation of the nodal amplitude factors; nodal angles; and astronomical arguments; for the
385 representative tidal constituents.

386 As the second step, under the 'credo of smoothness' assumption that the admittance or 'ratio of output to input' does not
387 change significantly between constituents of the same species (Munk and Cartwright, 1966; Pugh and Woodworth, 2014), the
388 amplitude ratio and phase lag difference of each representative tidal constituent for each tidal species between the temporary
389 and reference stations were calculated from the results of tidal harmonic analyses of concurrent 25 hr data slices (starting at

390 00.00) from the temporary observation and reference tidal stations (i.e. from SH_o and SH_r). The process of selecting the optimal
391 25 hr window for the concurrent data slices from amongst the 17.04 days of available records is explained in Sect. 3.
392 Once this 2017 window was selected, the third step involved adjusting the tidal predictions at the reference station calculated
393 from Eq. (A1), to represent those for the temporary station ($\eta_o(\tau)$), by substituting the daily (i.e. SH_o and SH_r) amplitude ratios
394 $\left(\frac{a_o^{(s)}}{a_r^{(s)}}\right)$ and phase lag differences $(G_o^{(s)} - G_r^{(s)})$ for the tidal constituents (K_1 and M_2) representing the diurnal and semidiurnal
395 tidal species between the temporary and reference stations into Eq. (A1) as follows (Byun and Hart, 2015):

$$396 \quad \eta_o(\tau) = \sum_{s=1}^k A_o^{(s)}(\tau) \cos\left(\omega_R^{(s)} t - \varphi_o^{(s)}(\tau)\right) \quad (A4)$$

$$397 \quad \text{with } A_o^{(s)}(\tau) = A_r^{(s)}(\tau) \left(\frac{a_o^{(s)}}{a_r^{(s)}}\right), \text{ and} \quad (A5)$$

$$398 \quad \varphi_o^{(s)}(\tau) = \varphi_r^{(s)}(\tau) + G_o^{(s)} - G_r^{(s)} \quad (A6)$$

399 Substituting Eqs. (A5) and (A6) into Eq. (A4), $\eta_o(\tau)$ can be expressed as:

$$400 \quad \eta_o(\tau) = \sum_{s=1}^k A_r^{(s)}(\tau) \left(\frac{a_o^{(s)}}{a_r^{(s)}}\right) \cos\left[\omega_R^{(s)} t - (\varphi_r^{(s)}(\tau) + G_o^{(s)} - G_r^{(s)})\right] \quad (A7)$$

401

402 The T_TIDE based CTSM code is available from https://au.mathworks.com/matlabcentral/fileexchange/73764-ctsm_t_tide.

403 **Author contribution**

404 D-SB conceived of the tidal prediction idea behind this paper, and drafted initial results sections. Both authors worked on
405 initial and final versions of the full manuscript.

406 **Competing interests**

407 The authors declare that the research was conducted in the absence of any commercial or financial relationships that could be
408 construed as a potential conflict of interest.

409 **Special issue statement (will be included by Copernicus)**

410 **Acknowledgements**

411 We are grateful to Land Information New Zealand (LINZ), and the Hydrographic Survey Division of the Korea Hydrographic
412 and Oceanographic Agency (KHOA), for supplying the tidal data used in this research. A special thank you to Glen Rowe
413 from LINZ for sharing his extensive knowledge of the Cape Roberts sea level gauge site and its records, and to a KHOA
414 colleague for providing the Fig. 1 photograph. Further, we gratefully thank Ms. Hyowon Kim at KHOA for her kind assistance
415 with drafting figures. We are also grateful to Philip Woodworth, Glen Rowe and an anonymous reviewer for comments that
416 greatly helped us improve our manuscript.

417 **References**

- 418 Byun, D.-S. and Hart, D. E.: On robust multi-year tidal prediction using T_TIDE, *Ocean Sci. J.*, 54, 685-691,
419 doi.org/10.1007/s12601-019-0028-4, 2019.
- 420 Byun, D.-S. and Hart, D. E.: Predicting tidal heights for new locations using 25h of in situ sea level observations plus reference
421 site records: A complete tidal species modulation with tidal constant corrections, *J. Atmos. Ocean. Tech.*, 32, 350-371,
422 doi.org/10.1175/JTECH-D-14-00030.1, 2015.
- 423 Carrère L., Lyard, F., Cancet, M., Guillot, A. and Picot, N.: FES 2014, a new tidal model - validation results and perspectives
424 for improvements, Presentation to ESA Living Planet Conference, Prague, 2016.
- 425 Codiga, D. L.: Unified Tidal Analysis and Prediction Using the UTide Matlab Functions, Technical report 2011-01, Graduate
426 School of Oceanography, University of Rhode Island, 2011.
- 427 Foreman, M. G. G.: Manual for Tidal Heights Analysis and Prediction, Pacific Marine Science Report, 77-10, 1977.
- 428 Gandolfi, S.: Terra Nova Bay Permanent Tide Gauge Observatory Site,
429 https://www.geoscience.scar.org/geodesy/perm_ob/tide/terranova.htm, last access 4 Feb. 2020, 1996.
- 430 Han, H. and Lee, H.: Glacial and tidal strain of landfast sea ice in Terra Nova Bay, East Antarctica, observed by interferometric
431 SAR techniques, *Remote Sens. Environ.*, 209, 41–51, doi.org/10.1016/j.rse.2018.02.033, 2018.
- 432 Han, H., Lee, J., and Lee, H.: Accuracy assessment of tide models in Terra Nova Bay, East Antarctica, for glaciological studies
433 of DDInSAR technique, *Korean Journal of Remote Sensing*, 29, 375–387, 2013.
- 434 Han, S. C., Shum, C. K., and Matsumoto, K.: GRACE observations of M2 and S2 ocean tides underneath the Filchner-Ronne
435 and Larsen ice shelves, Antarctica, *Geophys. Res. Lett.*, 32, L20311, doi.org/10.1029/2005GL024296, 2005.
- 436 Jourdain, N. C., Molines, J.-M., Le Sommer, J., Mathiot, P., Chanut, J., de Lavergne, C., and Madec, G.: Simulating or
437 prescribing the influence of tides on the Amundsen Sea ice shelves, *Ocean Model.*, 133, 44–55,
438 doi.org/10.1016/j.ocemod.2018.11.001, 2018.

439 King, M. A., Padman, L., Nicholls, K., Clarke, P. J., Gudmundsson, G. A., Kulesa, B., and Shepherd, A.: Ocean
 440 tides in the Weddell Sea: New observations on the Filchner-Ronne and Larsen C ice shelves and model validation, *J. Geophys.*
 441 *Res.*, 116, C06006, doi.org/10.1029/2011JC006949, 2011.
 442 LINZ, Land Information New Zealand: Sea level data downloads, [http://www.linz.govt.nz/sea/tides/sea-level-data/sea-level-](http://www.linz.govt.nz/sea/tides/sea-level-data/sea-level-data-downloads)
 443 [data-downloads](http://www.linz.govt.nz/sea/tides/sea-level-data/sea-level-data-downloads), last access 2019.
 444 Munk, W. H. and Cartwright, D. E.: Tidal spectroscopy and prediction, *Math. Phys. Sci.*, 259, 533-581,
 445 doi.org/10.1098/rsta.1966.0024, 1966.
 446 Padman, L., Erofeeva, S., and Fricker, H.: Improving Antarctic tide models by assimilation of ICESat laser altimetry over ice
 447 shelves, *Geophys. Res. Lett.*, 35, 122504, doi.org/10.1029/2008GL035592, 2008.
 448 Padman, L., Erofeeva, S., and Joughin, I.: Tides of the Ross Sea and Ross Ice Shelf cavity, *Antarct. Sci.*, 15, 31–40,
 449 doi.org/10.1017/S0954102003001032, 2003.
 450 Padman, L., Fricker, H., Coleman, R., Howard, S., and Erofeeva, L.: A new tide model for the Antarctic ice shelves and seas,
 451 *Ann. Glaciol.*, 34, 247–254, doi.org/10.3189/172756402781817752, 2002.
 452 Padman, L., Siegfried, M., and Fricker, H.: Ocean Tide Influences on the Antarctic and Greenland Ice Sheets, *Rev. Geophys.*,
 453 56, 142–184, doi.org/10.1002/2016RG000546, 2018.
 454 Pawlowicz, R., Beardsley, B., and Lentz, S.: Classical tidal harmonic analysis including error estimates in MATLAB using
 455 T_TIDE, *Comput. Geosci.*, 28(8), 929-937, doi.org/10.1016/S0098-3004(02)00013-4, 2002.
 456 Pugh, D. T.: Tides, Surges and Mean Sea-Level: A Handbook for Engineers and Scientists, Wiley, Chichester, United
 457 Kingdom, 1987.
 458 Pugh, D. T. and Woodworth, P. L.: Sea-level science: Understanding tides, surges, tsunamis and mean sea-level changes,
 459 Cambridge University Press, United Kingdom, doi.org/10.1080/00107514.2015.1005682, 2014.
 460 Rignot, E., Padman, L., MacAyeal, D., and Schmeltz, M.: Observation of ocean tides below the Filchner and Ronne Ice
 461 Shelves, Antarctica, using synthetic aperture radar interferometry: Comparison with tide model predictions, *J. Geophys. Res.-*
 462 *Oceans*, 105, 19615–19630, doi.org/10.1029/1999JC000011, 2000.
 463 Rosier, S. H. R. and Gudmundsson, G. H.: Tidal bending of ice shelves as a mechanism for large-scale temporal variations in
 464 ice flow, *The Cryosphere*, 12, 1699–1713, doi.org/10.5194/tc-12-1699-2018, 2018.
 465 Wild, C. T., Marsh, O. J., and Rack, W.: Differential interferometric synthetic aperture radar for tide modelling in Antarctic
 466 ice-shelf grounding zones, *The Cryosphere*, 13(12), 3171-3191, doi.org/10.5194/tc-13-3171-2019, 2019.

467 **Table 1. Major tidal harmonic results for diurnal and semidiurnal constituents from harmonic analyses of sea level observations:**
 468 **the year-long (2013) record from Cape Roberts (ROBT), and 17.04 day record (29 Jan. to 15 Feb. 2017) and 20.54 day record (29**
 469 **Dec. 2018 to 18 Jan. 2019) from Jang Bogo Antarctic Research Station (JBARS) in the Ross Sea (see source details in Sect. 2). For**
 470 **the JBARS tidal harmonic analyses, the inference method was used to infer the P_1 constituent from the K_1 , and the K_2 constituent**
 471 **from the S_2 , with their amplitude ratios and phase lag differences obtained from harmonic analysis of the long-term ROBT 2013**
 472 **reference station record.**

Tidal constituents & characteristics		ROBT (2013) 369 days		JBARS (2017) 17.04 days		JBARS (2019) 20.54 days	
		Amp. (cm)	Pha. (°)	Amp. (cm)	Pha. (°)	Amp. (cm)	Pha. (°)
Diurnal	O_1	21.1	202	19.6	208	16.0	208
	K_1	20.5	217	16.3	214	14.9	216
	P_1	6.6	215	5.2	213	4.8	214
	Q_1	4.4	190	-	-	-	-
Semidiurnal	M_2	5.3	5	6.7	4	6.3	34
	S_2	4.9	309	6.4	329	5.7	320
	N_2	3.8	255	-	-	-	-
	K_2	1.8	315	2.4	333	2.4	328
F		4.1 (diurnal form)		2.7 (mixed, mainly diurnal)		2.6 (mixed, mainly diurnal)	
ADI (day)		0.57		0.23		0.30	
AT (day)		-2.30		-1.44		-2.87	

473 **Note:** Amp. denotes amplitude; Pha. denotes phase lag, referenced to 0° Greenwich; F is the amplitude ratio of the ($K_1 + O_1$)/($M_2 +$
 474 S_2) tides; and ADI and AT denote the age of diurnal inequality and the age of the tide.

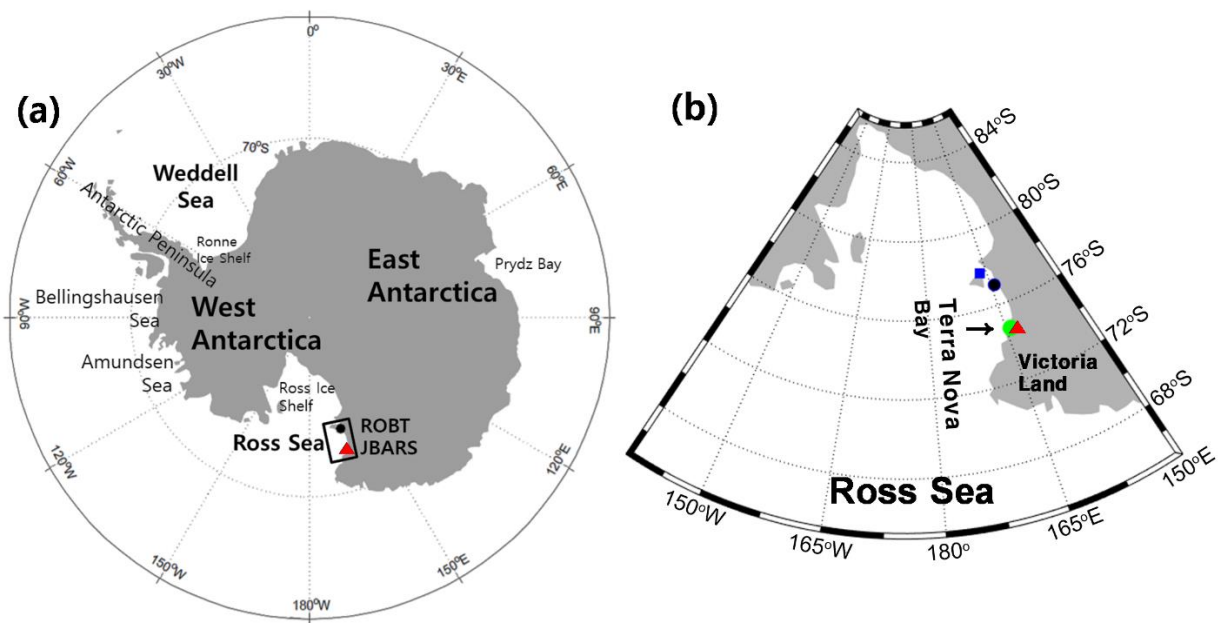
475 Table 2. Harmonic constants for 6 long-period tidal constituents, derived from harmonic analysis of [a](#) one year-long observations
 476 (2013) measured at the Cape Roberts sea level gauge (ROBT), using T_TIDEde (Pawlowicz et al., 2002). Note that this gauge is a
 477 vented piezometer so caution should be exercised in interpreting the results (particularly for S_a and S_{sa}) given the inclusion of
 478 proportionately large non-tidal (atmospheric) variations in this kind of sea level record

Constituent		Amplitude (cm)	Amplitude standard error (cm)	Phase lag (°)	Phase lag standard error (°)	SNR
Solar annual	S_a	5.8	4.8	75	50	1.5
Solar semi-annual	S_{sa}	0.1	3.3	352	194	0.06
Lunar monthly	MS_m	0.4	3.5	57	254	0.02
	M_m	2.9	3.8	139	102	0.59
Lunar fortnightly	MS_f	1.2	3.0	281	189	0.14
	M_f	2.7	3.9	153	101	0.47

479 Phase lags are referenced to 0° Greenwich, and SNR denotes the signal-to-noise ratios.

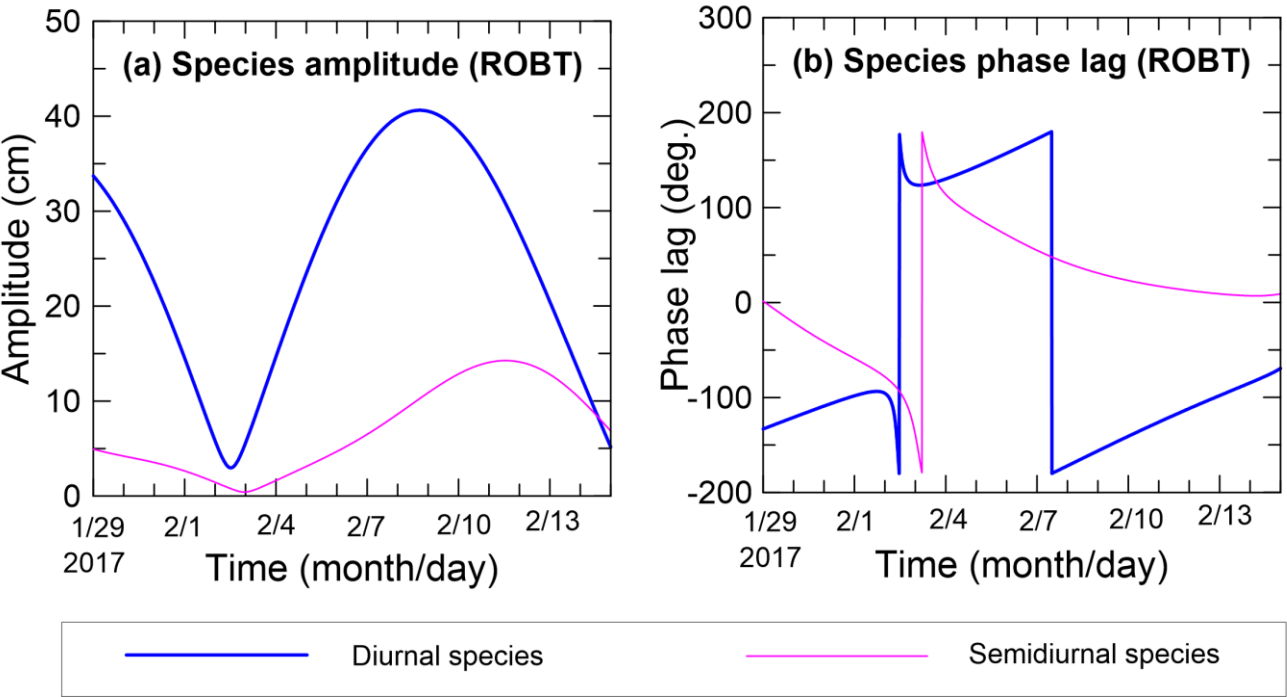


481
482 **Figure 1. Drifting ice, including icebergs and mobile sea ice, around the Jang Bogo Antarctic Research Station (JBARS),**
483 **photographed on 29 Jan. 2017.**



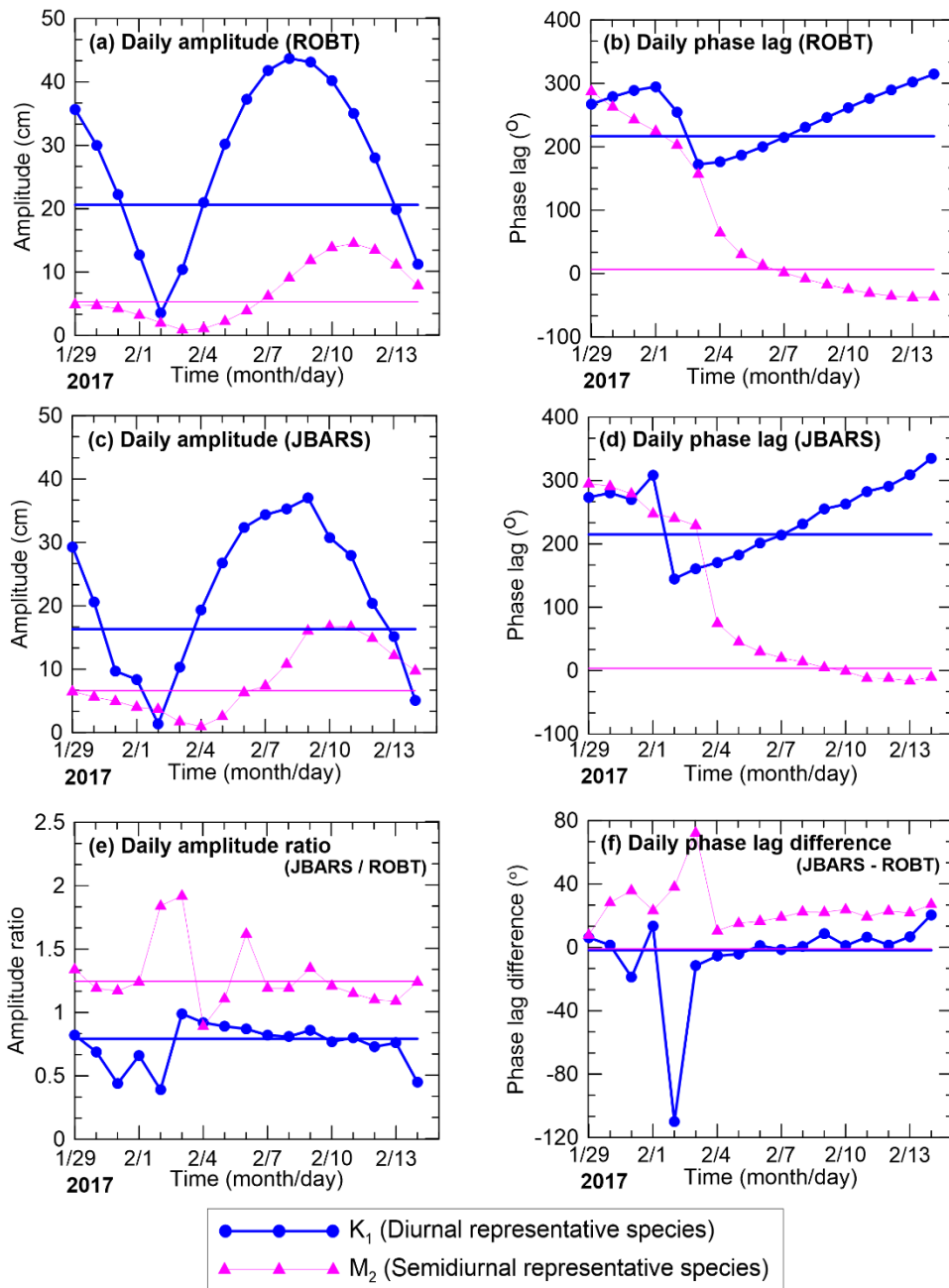
485

486 **Figure 2. Maps showing (a) the locations of the two tidal observation stations employed in this study within a wider Antarctic context:**
487 **Jang Bogo Antarctic Research Station (JBARS, ▲) and Cape Roberts (ROBT, ●); and (b) the case study station locations relative**
488 **to two other (previous) temporary tidal observations stations, McMurdo Station (■), and Mario Zucchelli Station (●), in the Ross**
489 **Sea.**



491

492 **Figure 3. Modulated tidal (a) species amplitudes and (b) phase lags for the diurnal and semidiurnal tidal species, calculated from**
493 **Cape Roberts (ROBT) tidal prediction data (29 Jan. to 14 Feb. 2017), using Appendix 1 Eqs. (A1) and (A3).**



494

495 **Figure 4. Daily amplitudes (a, c); phase lags (b, d); amplitude ratios (e); and phase lag differences (f) of the K_1 and M_2 tides**
 496 **(representative diurnal and semidiurnal tide species) at ROBT (a, b) and JBARS (c, d), and between JBARS and ROBT (e, f),**
 497 **calculated from ‘daily’ slices of the 29 Jan. to 14 Feb. 2017 ROBT tidal predictions and JBARS sea level observations. In addition,**
 498 **thick blue (K_1) and thin pink (M_2) horizontal lines in the panels indicate the amplitudes and phase lags derived from harmonic**
 499 **analyses of the entire 369 day 2013 ROBT sea level record (a, b) and of the entire 17 day 2017 JBARS sea level record (c, d), along**
 500 **with their amplitude ratios and phase lag differences (e, f).**

501

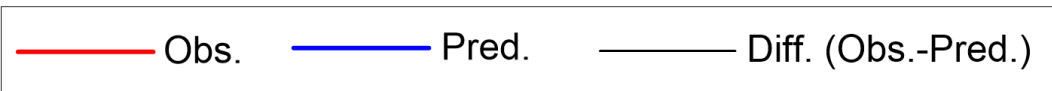
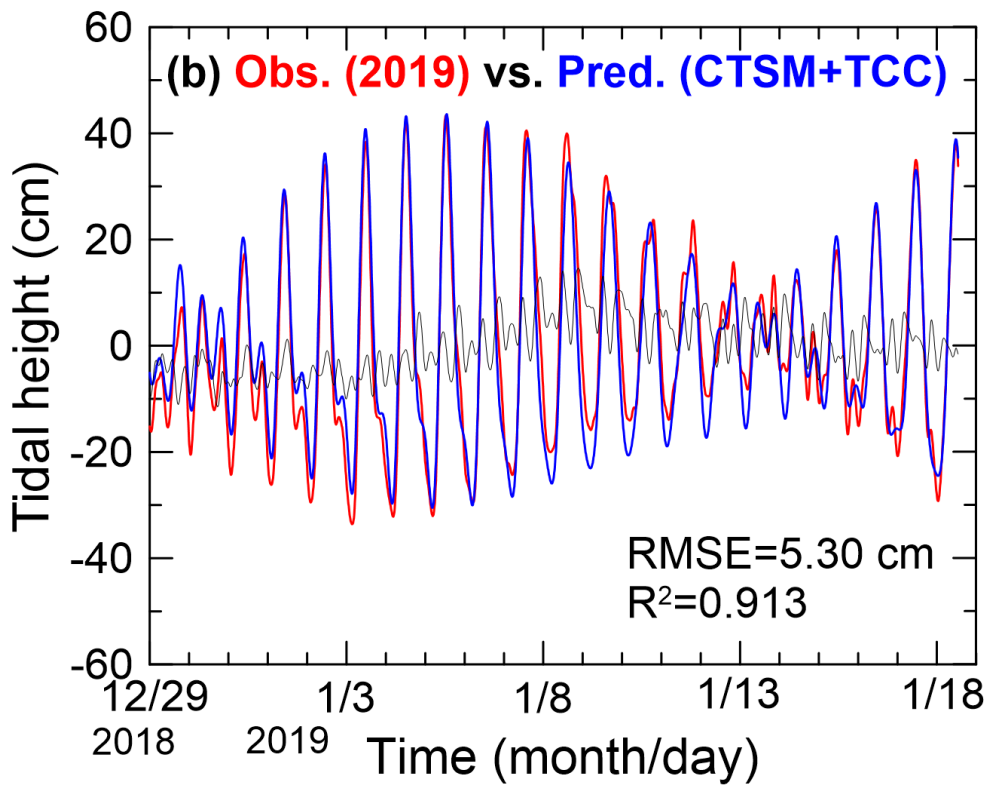
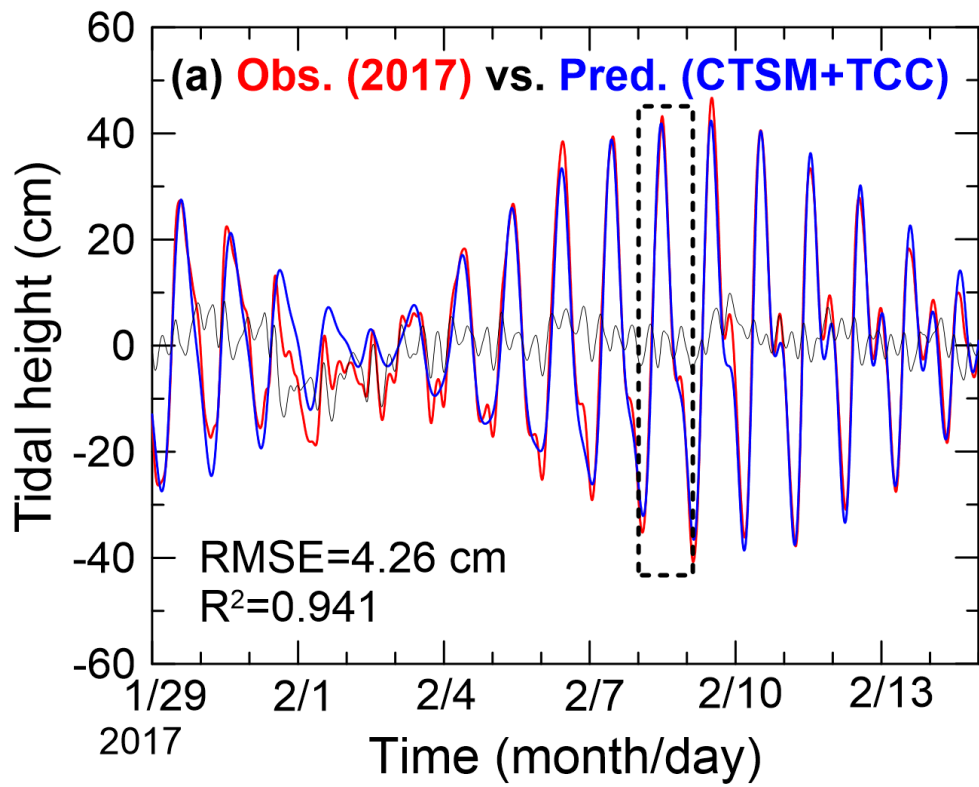
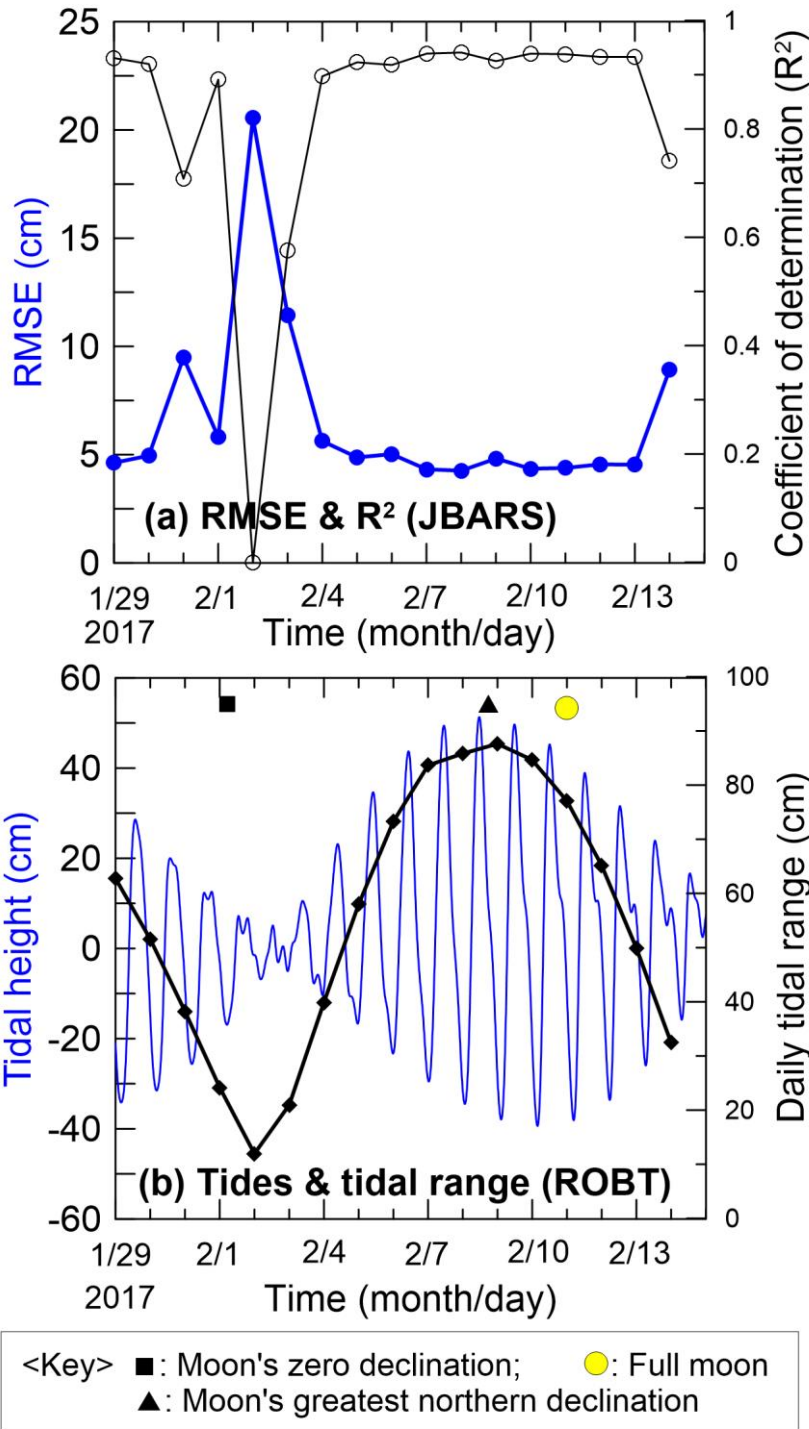


Figure 5. Time series of JBARS sea level observations (Obs.), predicted tidal heights (Pred.), and sea level residuals (Diff.) from (a) 29 Jan. to 14 Feb. 2017; and (b) 29 Dec. 2018 to 18 Jan. 2019. The JBARS predictions were generated via the CTSM+TCC method using a daily (25 hr) slice of local sea level observations from 8 Feb. 2017 (dashed box in (a)), along with concurrent (to time periods a and b) ROBT predictions; and year-long (2017) 5 min interval ROBT tidal predictions. RMSE and R² denote the comparison Root Mean Square Errors and coefficients of determination, respectively.

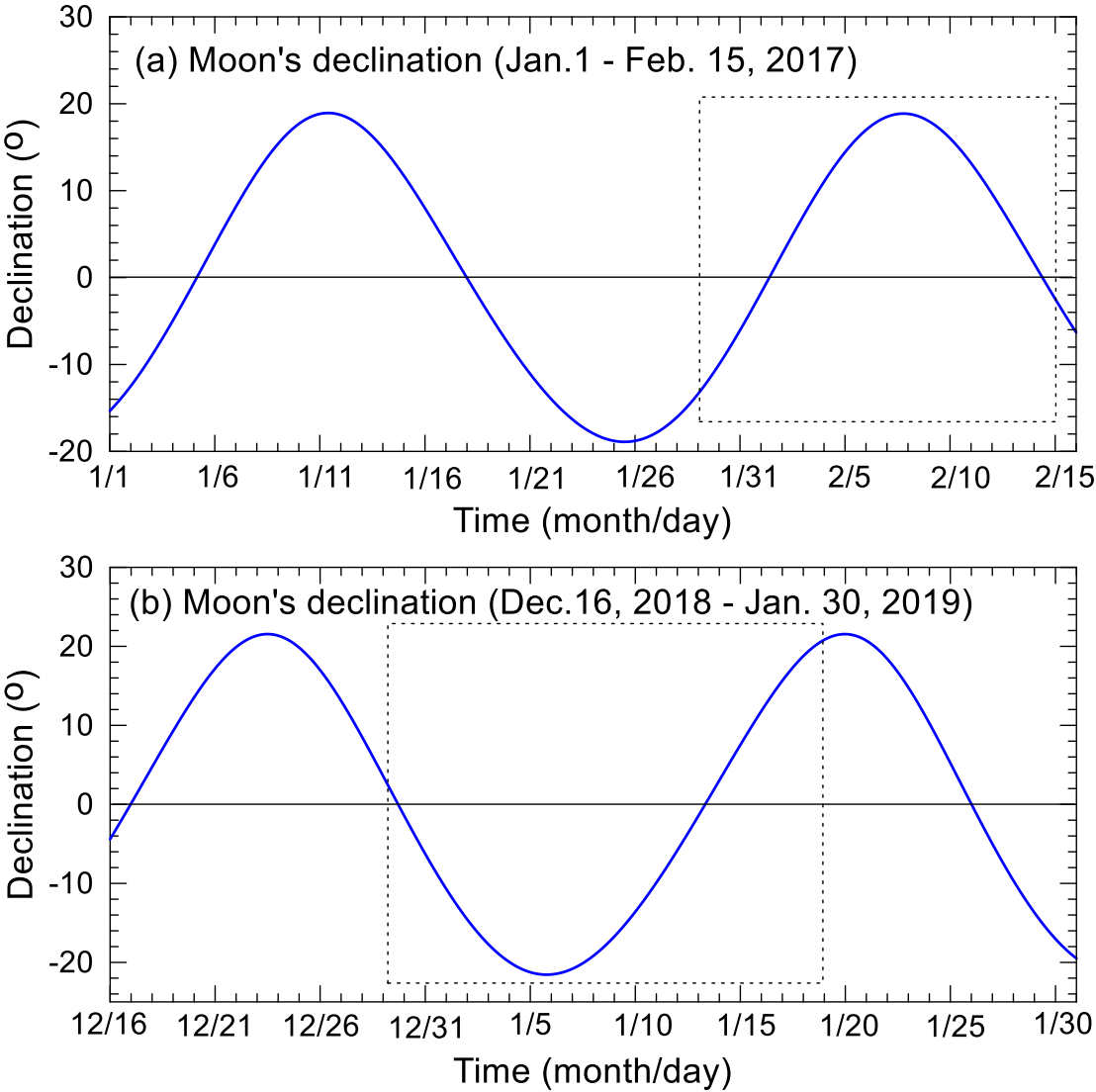


510

511 Figure 6. (a) Time series (29 Jan. to 14 Feb. 2017) of Root Mean Square Errors (RMSE, thick blue line with ●) and coefficients of
 512 determination (R², thin black line with ○) between JBARS 10 min interval sea level observations and the CTSM+TCC prediction
 513 datasets, generated for this site using harmonic analysis results from the JBARS daily (25 hr) sea level data slices and concurrent
 514 daily (25 hr) 2017 tidal prediction data slices and harmonic analysis results from ROBT station's year-long (2017) tidal predictions.
 515 (b) Time series of predicted 2017 tidal heights (thin blue line) and daily tidal ranges (thick black line with ♦) for ROBT, based on
 516 harmonic analysis of this station's 2013, 5 min interval sea level record, plus an indication of the moon's phase and declination.

517

518
519



520

521 **Figure 7. Time series of the Moon’s declination, calculated at daily intervals for two observation periods: (a) 1 Jan. to 15 Feb. 2017;**
522 **and (b) 16 Dec. 2018 to 30 Jan. 2019. Dashed boxes indicate the sea level observation windows examined in this study.**

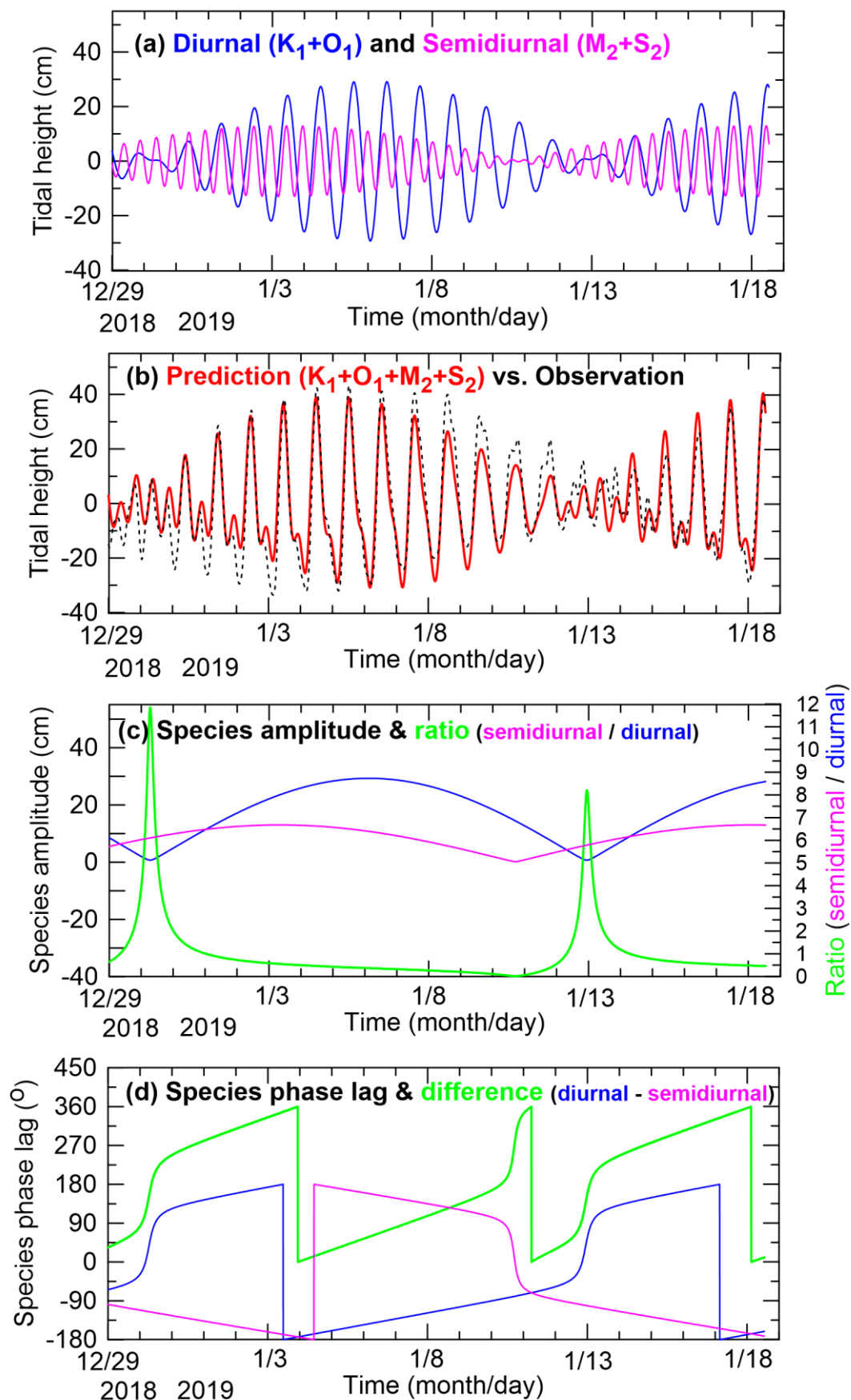
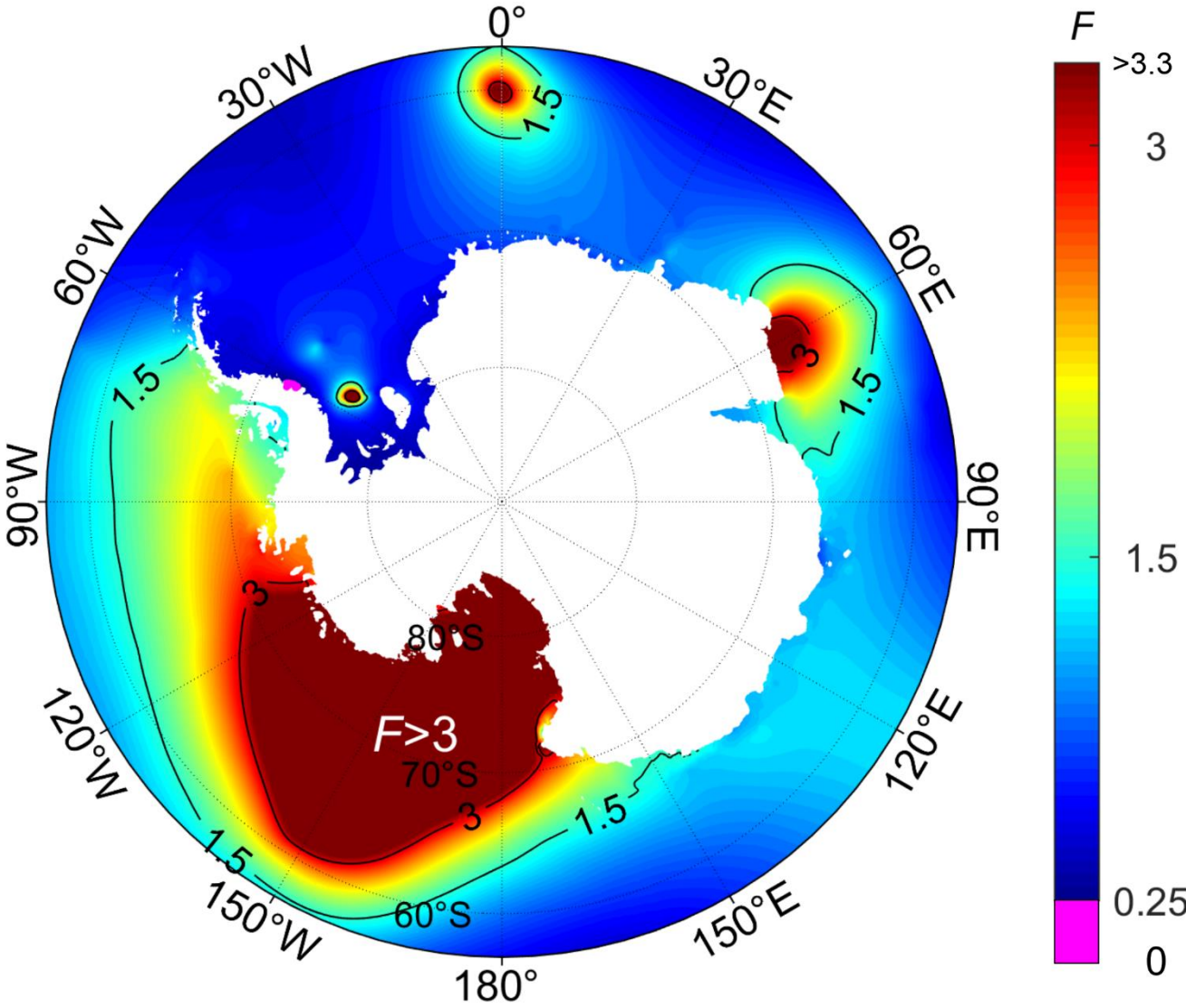


Figure 8. Time series (29 Dec. 2018 to 18 Jan. 2019) of (a) predictions of the diurnal (K_1+O_1) tides (blue line) and the semidiurnal (M_2+S_2) tides (magenta line) for JBARs; (b) their combined JBARs predictions (red line) and observations (black dashed line); (c) the ROBT diurnal (blue line) and semidiurnal (magenta line) species amplitudes and their ratio (green line); and (d) the ROBT diurnal (blue line) and semidiurnal (magenta line) species phase lags and their difference (diurnal – semidiurnal) (green line).



530 **Figure 9. Distribution of tidal form factor (F) values around Antarctica. Note the magenta area (72°S) on the Antarctic Peninsula's**
531 **Weddell Sea coast denotes the only area with a properly semidiurnal tide regime ($F < 0.25$) in the Antarctic region.**